



## Numerical investigation of the hump characteristic of a pump–turbine based on an improved cavitation model

Liu Jintao<sup>a,\*</sup>, Liu Shuhong<sup>b</sup>, Wu Yulin<sup>b</sup>, Jiao Lei<sup>a</sup>, Wang Leqin<sup>a</sup>, Sun Yuekun<sup>b</sup>

<sup>a</sup> Institute of Chemical Process Machinery, Zhejiang University, Hangzhou 310027, China

<sup>b</sup> State Key Laboratory of Hydrosience and Engineering, Tsinghua University, Beijing 100084, China

### ARTICLE INFO

#### Article history:

Received 23 April 2012

Received in revised form 26 July 2012

Accepted 1 August 2012

Available online 13 August 2012

#### Keywords:

Pump–turbine

Hump characteristics

SST  $k-\omega$  turbulence model

Improved cavitation model

### ABSTRACT

For the safe and stable operation of a pump–turbine at pump mode, the hump characteristics must be studied and the hump region should be avoided. 3-D (three dimensional), compressible, cavitating flows in a pump–turbine at pump mode were numerically studied using SST  $k-\omega$  turbulence model and mixture model. The decrease of the kinematic eddy viscosity in the region of high volume fraction of water vapor was considered in the calculation. The flow and external characteristic in the hump region were analyzed. Results show that the hump characteristic of a pump–turbine might be related to the cavity flow in the pump–turbine. It is the appearance of the cavitation that reduces the head of the pump–turbine. The cavitation incipience is thought to occur when the pump–turbine runs at the peak head and the cavitation is worse at 80% discharge of the pump–turbine. The cavitation regions locate at the inlet of the suction side. Calculation results are in good agreement with experimental data. The pressure fluctuation at the wave trough of hump characteristic is determined by the rotational speed. Numerical study of hump characteristics can provide a basic understanding for the improvement of stable operation of a pump–turbine.

© 2012 Elsevier Ltd. All rights reserved.

### 1. Introduction

The hump characteristic is one of the special characteristics of a pump–turbine at pump mode with small flow. Especially, when the pump–turbine runs at high head level, the hump region is unavoidable and the performance is reduced. If a pump–turbine runs in hump region, the flow is small and it may cause large pressure fluctuations. Strong noise can be heard during the starting period and the start time is prolonged [1]. Nowadays, the stability of a pump–turbine is more and more important, and it has become essential to study the parameters cause instable characteristics.

For investigation of the stability of pump–turbines, lots of researches have been done. Rodriguez et al. [2] investigated the rotor–stator interaction (RSI) of a pump–turbine through theoretical analysis incorporated the number of blades and guide vanes, the non-uniform fluid force, and the sequence of interaction. Ruchonnet et al. [3] and Nicolet and Ruchonnet [4] set up a one-dimensional hydroacoustic model to perform the numerical simulation of the RSI. Braun et al. [5] analyzed the change in the global performance at pump mode and it was related to a change of the secondary flow pattern in the diffuser channels. Ran et al. [6] studied the unsteady flow in a pump–turbine and presented an

improved runner to reduce the pressure fluctuation. Most studies were carried out on the pump–turbine within the unsteady RSI and phenomena of flow separation. The researches on the hump characteristic at pump mode were limited. The mechanism of the hump characteristic was still unknown.

The cavitation in a turbo-machinery may reduce the performance of the whole unit. Researches on the cavitation flow in turbo-machineries were a hot topic for the improvement of flow passage components [7–9], but the analysis of hump characteristics combined with the cavitation phenomenon have not yet been reported. Most of recent studies on pump–turbine at pump mode were carried out by single phase, and the reason for causing the hump characteristic is unclear. In this paper, a cavitation model was used to analyze the hump characteristic of a model pump–turbine by numerical simulation. The results based on unsteady calculations were compared with experimental data. The performance of the pump–turbine at pump mode, as well as the cavitation flow in the runner was analyzed.

### 2. Pump–turbine geometry

The study was performed with the model pump–turbine. Parameters of the prototype pump–turbine are shown in Table 1.  $D_1$  denotes the runner inlet diameter in pump mode;  $Z_s$ ,  $Z_G$  and  $Z$  are the numbers of stay vanes, guide vanes and runner blades,

\* Corresponding author.

E-mail addresses: [liujintao86@hotmail.com](mailto:liujintao86@hotmail.com) (J.T. Liu), [liushuhong@mail.tsinghua.edu.cn](mailto:liushuhong@mail.tsinghua.edu.cn) (S.H. Liu).

## Nomenclature

$D_1$	runner inlet diameter in pump mode (mm)	$Z_5$	number of stay vanes
$H_d$	the rated head (m)	$Z_G$	number of guide vanes
$H_{th}$	theoretical head of the pump–turbine	$c_u$	tangential velocity
$H_a$	atmospheric pressure head	$n$	rotational speed of the runner (rpm)
$H_{va}$	vacuum head in the draft tank of test rig	$t$	time (s)
$H_s$	suction head of the pump–turbine	$u_1$	peripheral speed at the inlet of the blade
$H_V$	vapor pressure head at the test temperature (25 °C)	$u_2$	peripheral speed at the outlet of the blade
$Q_d$	the rated discharge ( $\text{m}^3/\text{s}$ )		
$Q$	volume flow rate ( $\text{m}^3/\text{s}$ )		
$Z$	number of blades		

respectively;  $H_d$  denotes the rated head;  $n$  denotes the rotational speed of the runner;  $Q_d$  denotes the rated discharge.

The pump–turbine's structure is shown in Fig. 1. The relative opening ( $\gamma$ ) of guide vanes is 80%, which is used for the calculation of the pump–turbine.

## 3. Numerical method

### 3.1. Governing equations of mixture model

In this paper, a mixture model [10–12] is adopted for simulation of the cavitating flow through the pump–turbine. Since all phases share the same velocity, the governing equations are:

$$\frac{\partial \rho_m}{\partial t} + \frac{\partial}{\partial x_j} (\rho_m u_j) = 0 \quad (1)$$

$$\frac{\partial}{\partial t} (\rho_m u_i) + \frac{\partial}{\partial x_j} (\rho_m u_i u_j) = -\frac{\partial p}{\partial x_i} + \frac{\partial}{\partial x_j} \left[ (\mu + \mu_T) \left( \frac{\partial u_i}{\partial x_j} + \frac{\partial u_j}{\partial x_i} \right) \right] \quad (2)$$

$$\frac{\partial (\alpha_v \rho_v)}{\partial t} + \frac{\partial (\alpha_v \rho_v u_j)}{\partial x_j} = S \quad (3)$$

where the density  $\rho_m$  is defined through volume fractions as  $\rho_m = \alpha_l \rho_l + \alpha_v \rho_v$ .

$\rho_l$ ,  $\rho_v$  are the densities of liquid and non-dissolved gas, respectively;  $\alpha_l$ ,  $\alpha_v$  are the volume fractions of liquid and non-dissolved gas, respectively;  $\mu$  is the viscosity of mixture;  $\mu_T$  is the kinematic eddy viscosity of mixture, which is obtained via the following turbulence model;  $u_j$  is the velocity field calculated from the momentum equations;  $\tau_{ij}$  is the deformation tensor;  $S$  is the source term caused by cavitation.

### 3.2. Turbulence model

In this paper, the SST  $k$ - $\omega$  turbulence model was used to close the Reynolds averaged Navier–Stokes (RANS) solver for the solution of the two-phase turbulence flows.

$$\rho_m \frac{\partial k}{\partial t} + \rho_m u_j \frac{\partial k}{\partial x_j} = \frac{\partial}{\partial x_j} \left[ (\mu + \sigma_k \mu_T) \frac{\partial k}{\partial x_j} \right] - \beta^* \rho_m k \omega + P_k \quad (4)$$

**Table 1**  
Parameters of the model pump–turbine.

$H_d$ (m)	52.4
$Q_d$ ( $\text{m}^3/\text{s}$ )	0.45
$n$ (rpm)	1500
$D_1$ (m)	0.3
$Z$	9
$Z_5$	20
$Z_G$	20

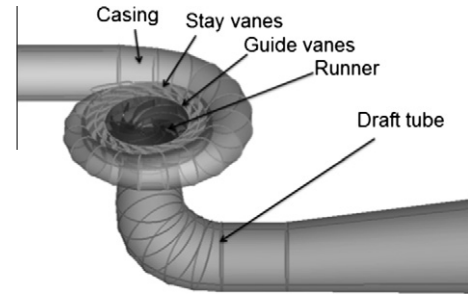


**Fig. 1.** Profile of pump–turbine.

$$\rho_m \left( \frac{\partial \varepsilon}{\partial t} + u_j \frac{\partial \varepsilon}{\partial x_j} \right) = \frac{\partial}{\partial x_j} \left[ (\mu + \sigma_\omega \mu_T) \frac{\partial \varepsilon}{\partial x_j} \right] + 2(1 - F_1) \sigma_{\omega 2} \frac{\rho_m}{\omega} \frac{\partial k}{\partial x_i} \frac{\partial \omega}{\partial x_i} - \rho_m (\alpha S^2 - \beta \omega^2) \quad (5)$$

Auxiliary relations are shown as follows,

$$P_k = \min \left( \tau_{ij} \frac{\partial u_i}{\partial x_j}, 10 \beta^* k \omega \right)$$

$$F_1 = \tanh \left\{ \left\{ \min \left[ \max \left( \frac{\sqrt{k}}{\beta^* \omega y}, \frac{500 \mu}{\rho_m y^2 \omega} \right), \frac{4 \sigma_{\omega 2}}{CD_{k\omega} y^2} \right] \right\}^4 \right\}$$

$$CD_{k\omega} = \max \left( 2 \rho \sigma_{\omega 2} \frac{1}{\omega} \frac{\partial k}{\partial x_i} \frac{\partial \omega}{\partial x_i}, 10^{-10} \right)$$

The closure coefficients are chosen as

$$\alpha = \frac{5}{9}, \quad \beta = 0.075, \quad \beta^* = 0.09, \quad \sigma_k = 0.85, \quad \sigma_{\omega 1} = 0.5, \quad \sigma_{\omega 2} = 856$$

### 3.3. Kinematic eddy viscosity

The kinematic eddy viscosity is obtained based on traditional Boussinesq hypothesis [13],

$$\mu_T = \rho_m C_\mu \frac{k^2}{\varepsilon} \quad (6)$$

The specific dissipation rate [14] is defined as:

$$\omega = \frac{\varepsilon}{C_k k} \quad (7)$$

where  $C_k = 1$ ,  $C_\mu = 0.09$ .

So the Eq. (6) can be written as,

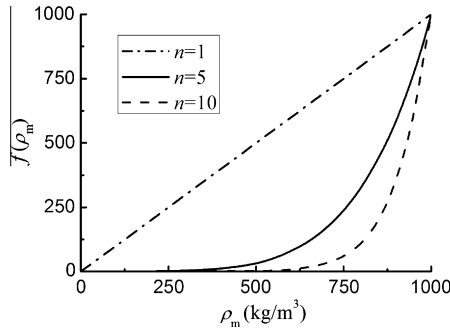


Fig. 2. The relation between  $f(\rho_m)$  and  $\rho_m$  [15].

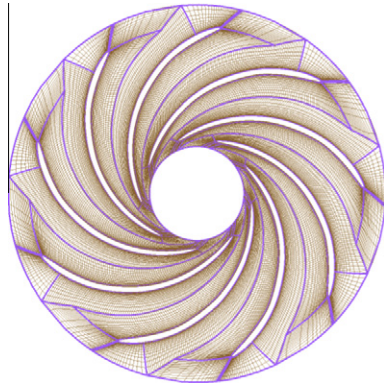


Fig. 3. Mesh of runner.

$$\mu_T = \rho_m c_\mu \frac{k}{\omega} \quad (8)$$

Considering the compressible mixture in the cavitating flow, a function  $f(\rho_m)$  [15,16] is introduced shown in Eqs. (9) and (10). The relation between  $f(\rho_m)$  and  $\rho_m$  is shown in Fig. 2. When  $n = 10$ , the application of  $f(\rho_m)$  can reduce the kinematic eddy viscosity coefficient in the region of high volume fraction of water vapor.

$$\mu_T = f(\rho_m) c_\mu k / \omega \quad (9)$$

$$f(\rho_m) = \rho_v + [(\rho_m - \rho_v) / (\rho_l - \rho_v)]^n \cdot (\rho_l - \rho_v) \quad (n = \text{constant and } n \geq 1) \quad (10)$$

So the kinematic eddy viscosity is

$$\mu_T = \{\rho_v + [(\rho_m - \rho_v) / (\rho_l - \rho_v)]^n \cdot (\rho_l - \rho_v)\} c_\mu k / \omega \quad (n = \text{constant and } n \geq 1) \quad (11)$$

In this calculation,  $n = 10$  was used for the simulation of cavitating flow in the pump-turbine.

### 3.4. Compressible cavitation model

The Rayleigh Plesset model was used to model cavitation in the pump-turbine. It provided the basis for the rate equation controlling vapor generation and condensation. The homogeneous multi-phase model with two fluids, water and water vapor was employed. Cavitation was treated without thermal phase change. The interphase mass transfer rate was calculated by the solver.

The condensation was included as follows:

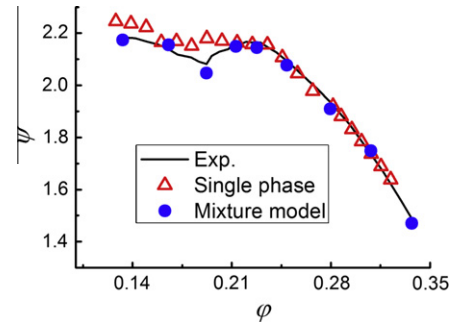


Fig. 4. Hump characteristic of the pump-turbine.

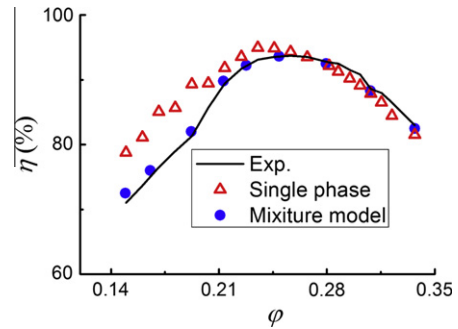


Fig. 5. Efficiency of the pump-turbine.

$$\dot{m} = F_{cond} \frac{3\alpha_v \rho_v}{R_B} \sqrt{\frac{2|p_v - p|}{3\rho_l}} \text{sgn}(p_v - p) \quad (12)$$

For vaporization:

$$\dot{m} = F_{vap} \frac{3\alpha_v (1 - \alpha_v) \rho_v}{R_B} \sqrt{\frac{2|p_v - p|}{3\rho_l}} \text{sgn}(p_v - p) \quad (13)$$

where  $F_{cond} = 0.01$  and  $F_{vap} = 50$  were empirical factors for condensation and vaporization, respectively;  $R_B = 1 \mu\text{m}$ ;  $p_v$  was the saturated vapor pressure.

In order to consider the change of water density during the calculation of cavitation, Venkateswaran et al. [17] and Yan et al. [18] used the state equation in transport equations, and the external characteristic has been proved more accurate compared with experimental data. The state equation is shown as follows,

$$\rho_l = \rho_o + \frac{p - p_f}{a^2} \quad (14)$$

where  $\rho_l$  is the water density;  $\rho_o = 998.2 \text{ kg/m}^3$  is the reference density of water;  $p_f = 101325 \text{ Pa}$  is the reference pressure of water;  $a = 1400 \text{ m/s}$  is the sound speed.

Eq. (14) is used in the calculation of cavitating flow in the paper. The void fraction ( $5 \times 10^{-5}$ ) of the nuclei is used in the simulation for the prediction of cavitation inception.

### 3.5. Simulation conditions

The parameter to express the operating condition of the pump-turbine at pump mode is the cavitation number,  $\sigma$ , obtained by

$$\sigma = \frac{H_a - H_{va} - H_s - H_v}{H} \quad (15)$$

where  $H_a$  is the atmospheric pressure head;  $H_{va}$  is the vacuum head in the draft tank of test rig, which indicates the pressure level at the

outlet of draft tube;  $H_s$  is the suction head of the pump–turbine;  $H_v$  is the vapor pressure head at the test temperature (25 °C).

The cavitation number were chosen in the range of 0.25–0.27 according to the model test. Velocity at draft tube inlet was specified at pump mode. At the casing outlet, the global conservation of mass was to be fulfilled. The outlet condition was chose and the value of static pressure was used. No slip wall boundary condition in the solid walls was specified. The runner’s hydraulic region was set to rotate at a speed of 1500 rpm. The upwind discretization scheme was used to discretize the advection term. In order to reduce  $y^+$  of the solid walls, 8 mesh layers on solid walls were used. Mesh grids of the runner is shown in Fig. 3. The time step was 0.0001 s. Thus, the converged turbulent flow solutions were obtained by rotating the mesh in the runner region by 1° per time step. The unsteady solutions are formed by the converged solutions at all times. During the unsteady calculation, the pressure and velocity change with time in the whole flow passage.

## 4. Results and discussion

### 4.1. Performance of the pump–turbine

In order to study the hump characteristic, the pump–turbine within the flow rate levels of  $Q/Q_D = 0.5–1.2$  were calculated by single phase flow and mixture model, respectively. Both of the two models are calculated by unsteady calculation. Results of the total head coefficient  $\psi$  are shown in Fig. 4.

The flow coefficient  $\varphi$ , and total head coefficient  $\psi$  are defined as follows,

$$\varphi = \frac{Q}{\pi\omega_0 R^3} \quad (16)$$

$$\psi = \frac{2gH}{\omega_0^2 R^2} \quad (17)$$

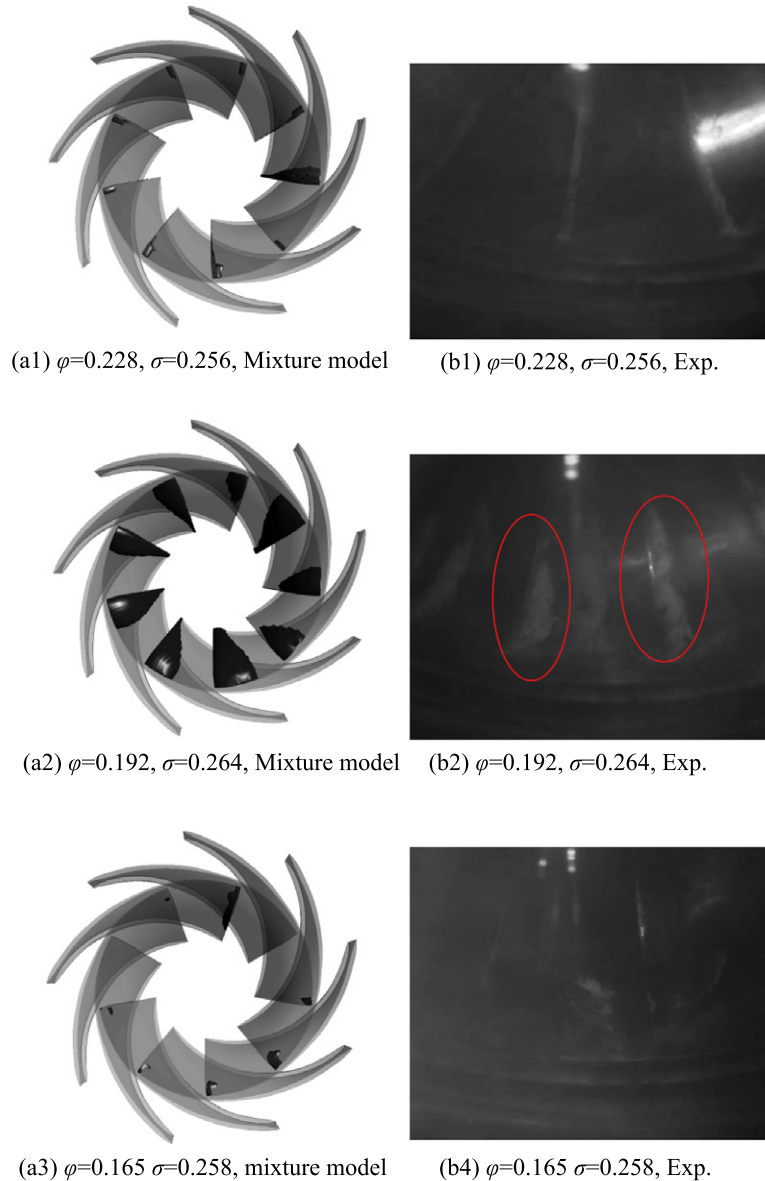


Fig. 6. Cavitation in the runner.

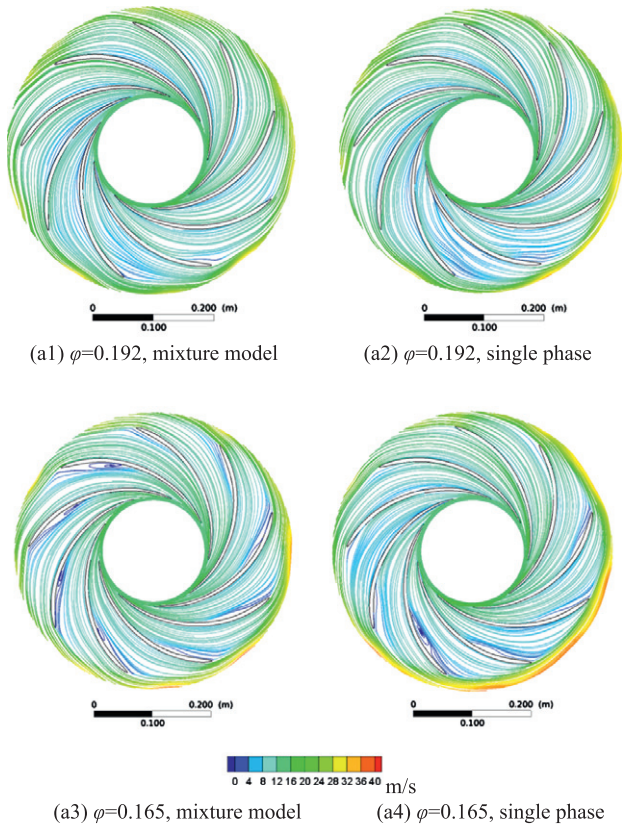


Fig. 7. Streamlines on the blade to blade surface.

where  $Q$  is the flow rate,  $R$  is the radius of outlet of the runner,  $\omega_0$  is the rotational speed of the runner,  $H$  is the head of the pump-turbine,  $g$  is the acceleration of gravity.

Results show that the calculation result based on cavitation model agrees well with the experiment data, while the result based on single phase flow has large error at the trough of the hump characteristic. The error of  $\psi$  based on the single flow model is 0.2 at the trough of wave. The result of single phase model could not calculate the reduction of  $\psi$  in the range of  $\varphi = 0.17\text{--}0.22$ .

Fig. 5 shows the efficiency of the pump-turbine in the calculating range. This pump-turbine has high efficiency (93%) in the range of  $\varphi = 0.22\text{--}0.28$ . Results based on single phase model have large error compared with experimental data when  $\varphi = 0.17\text{--}0.22$ . Results calculated by mixture model agree well with experimental data in the whole calculating range. When the pump-turbine runs in the hump region, the efficiency decreases greatly. The single phase can be used in the calculation of the operating range rather than the hump

region. The energy loss caused by vanes and casing calculated by single phase is about 6.3%, which is very close to 5.5% calculated by mixture model, and the difference only causes  $\psi$  higher than the result of mixture model by 0.02. The energy loss in the vane is not the main reason caused the hump characteristic.

#### 4.2. Cavitation analysis at pump mode

The outlet pressure was specified according to the parameter  $\sigma$  of the experiment. The cavitating flow was calculated by mixture model. Results of the cavitation in the runner are shown in Fig. 6. The boundary of the cavitating region is settled according to the volume fraction of cavity is 10%, which was proposed by Okita and Kajishima [19]. When the pump-turbine runs at operating range ( $\varphi = 0.27\text{--}0.33$ ), no-cavitating flow can be seen in the pump-turbine. As the flow rate decreases, the pressure at the inlet of the suction side of the runner reduces to the saturated vapor pressure. The cavitation in the runner occurs when  $\varphi$  is 0.228. In the range of  $\varphi = 0.192\text{--}0.228$ , the cavitation region increases as  $\varphi$  decreases and cavitation is the most serious when  $\varphi$  is 0.192. It might be the reason caused the reduction of the head of the pump-turbine. The hump characteristic might be attributed to the appearance of cavitation in the runner. In the range of  $\varphi = 0.165\text{--}0.192$ , the cavitating flow gradually disappears as  $\varphi$  decreases. No cavitating flow in the runner when  $\varphi < 0.16$ . The cavitating flow in the pump-turbine rotates fixed to the runner. Cavitating flows in the runner are also proved by the experiment result shown in Fig. 6b.

#### 4.3. Flow distribution in the pump-turbine

Streamlines on the blade to blade surface are shown in Fig. 7. Flow in the runner of the single phase model are almost the same to the result of mixture model when  $\varphi \geq 0.192$ , and there is no vortex in the pump-turbine. The appearance of cavitation at  $\varphi = 0.192$  might not destroy the uniform flow in the pump-turbine. More vortexes in the suction side of the runner are obtained based on mixture model when  $\varphi < 0.192$ . Although streamlines in the runner have only a little difference, the pressure distribution on the blade surface is changed greatly for mixture model, which is shown in Fig. 8. The pressure level of the mixture model at the outlet of the runner is higher than the result of single phase. The minimum pressure calculated by single phase is smaller than the saturated vapor pressure. Fig. 9 shows streamlines in the region of the casing and vanes. Both of the two models can obtain the stall phenomenon in the region between guide vanes and stay vanes.

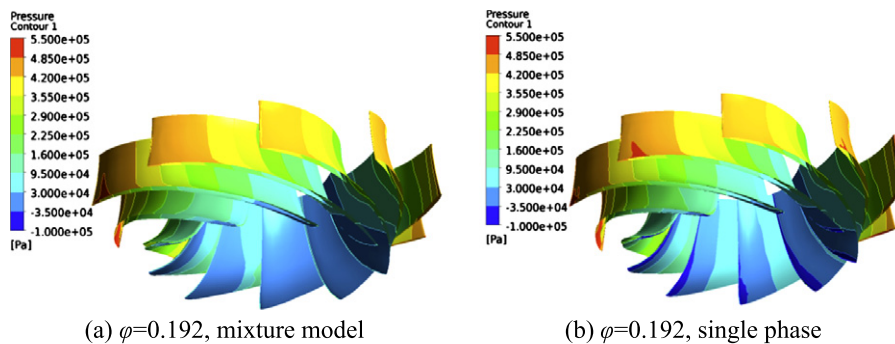


Fig. 8. Pressure on the blade surface (Pa).

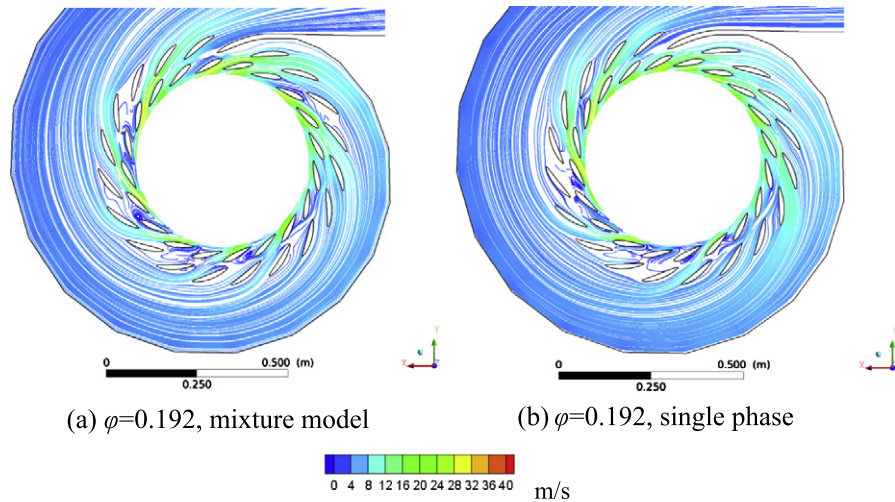


Fig. 9. Streamlines on the  $z = 0$  mm surface.

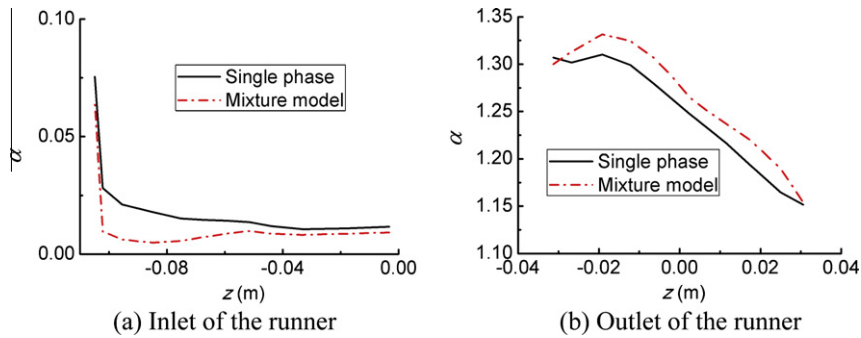


Fig. 10. Non-dimensional velocity circulation.

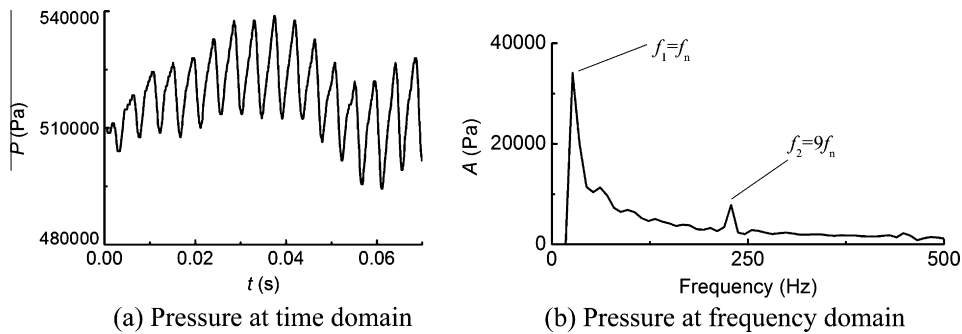


Fig. 11. Pressure fluctuation between runner and guide vanes.

4.4. Non-dimensional velocity circulation

A parameter  $\alpha$  is specified to analyze the distribution of energy of the runner. The parameter  $\alpha$  comes from the Euler Eq. (5), which is a non-dimensional energy can be calculated by Eq. (19).

$$H_{th}g = u_1c_{u1} - u_2c_{u2} \tag{18}$$

$$\alpha = uc_u/H_dg = (2\pi rc_u)n_0/H_dg \tag{19}$$

$H_{th}$  is the theoretical head of the pump–turbine.  $u_1$  is the peripheral speed at the inlet of the blade,  $u_2$  is the peripheral speed at the out-

Table 2  
Relative amplitude and dominant frequency.

	Mixture model	Experiment
$\Delta H/H$ (%)	10.8	13.2
Dominant frequency $\times f_n$ (Hz)	1	1

let of the blade,  $c_u$  is the tangential velocity,  $u = 2\pi rn_0$  is the peripheral speed,  $2\pi rc_u$  is the velocity circulation.

When  $\varphi = 0.192$ , results of  $\alpha$  at the inlet and outlet of the runner along  $z$  axis are shown in Fig. 10. From the comparison between

the result of single phase and mixture model, it can be concluded that the cavitating flow not only increases  $\alpha$  at the outlet of the runner, but also decreases  $\alpha$  at the inlet. The appearance of cavitation may block the passage in the runner, which increases the energy loss in the runner.

#### 4.5. Pressure fluctuations when $\varphi = 0.19$

When the pump–turbine runs in hump region, the amplitude of pressure fluctuation rises greatly. To study the instability of the pump–turbine when cavitation occurs in the runner, the pressure fluctuation between the runner and guide vane is calculated by mixture model and shown in Fig. 11. The dominant frequency of the pressure is the rotational frequency of the runner. The amplitude of pressure at dominant frequency is about 70% of the amplitude of the pressure fluctuation, so the pressure fluctuation is mainly determined by the rotational speed. It might be caused by the non-uniform cavitating flow (shown in Fig. 6) in the runner rotates fixed to the runner and the non-uniform structure of the casing in the pump–turbine. The blade passing frequency ( $9f_n$ ) is also obtained. The relative amplitude ( $\Delta H/H$ ) and dominant frequency at the point between runner and guide vanes is shown in Table 2. It can be concluded that the calculation result of mixture model is in good agreement with experimental data.

## 5. Conclusions

The study of hump characteristics for pump–turbine is essential for the operation of a pumped storage power plant. The calculation results using SST  $k-\omega$  model based on compressible cavitation model are in good agreement with experimental data. The calculation using single phase could not obtain accuracy result of the hump characteristic. The hump characteristic might be attributed to the appearance of cavitation at the inlet of suction side of the runner. The pressure fluctuation when the cavitation is serious is mainly depended on the rotational speed.

Further study will focus on the mechanism of cavitation, and improvement of the hump characteristics of the pump–turbine.

## Acknowledgments

The authors would like to thank National Natural Science Foundation of China (Nos. 51006087, 51076077) and the project supported by National Science and Technology Ministry (ID: 2011BAF03B01) for their financial support.

## References

- [1] Mei ZY. Power generation technology of pumped storage power station. China Machine Press; 2000. p. 200–21 [in Chinese].
- [2] Rodriguez CG, Egusquiza E, Santos IF. Frequencies in the vibration induced by the rotor stator interaction in a centrifugal pump turbine. *J Fluid Eng* 2007;129:1428–35.
- [3] Ruchonnet N, Nicolet C, Avellan F. Hydroacoustic modeling of rotor stator interaction in Francis pump–turbine. In: IAHR int. meeting of WG on cavitation and dynamic problems in hydraulic machinery and systems, Barcelona; 2006.
- [4] Nicolet C, Ruchonnet N. Hydroacoustic simulation of rotor–stator interaction in resonance conditions in Francis pump turbine. *IOP Conf Ser: Earth Environ Sci* 2010;12:012005-1–5-9.
- [5] Braun O, Kueny JL, Avellan F. Numerical analysis of flow phenomena related to the unsteady energy-discharge characteristic of a pump–turbine in pump mode. In: ASME fluids engineering division summer meeting and exhibition, Houston, TX, USA; 2005. P. 1–6.
- [6] Ran HJ, Luo XW, Zhang Y. Numerical simulation of the unsteady flow in a high-head pump–turbine and the runner improvement. In: Proceedings of FEDSM 2008, ASME fluids engineering conference, 2008, Jacksonville, Florida, USA; 2008.
- [7] Fortes-Patella R, Coutier-Delgosha O, Perrin J, Reboud JL. Numerical model to predict unsteady cavitating flow behavior in inducer blade cascades. *J Fluid Eng* 2007;129:128–35.
- [8] Lindau JW, Kunz RF, Boger DA, Stinebring DR, Gibeling HJ. High Reynolds number, unsteady, multiphase CFD modeling of cavitating flows. *J Fluid Eng* 2002;124:607–16.
- [9] Medvitz RB, Kunz RF, Boger DA, Lindau JW, Yocum AM, Pauley LL. Performance analysis of cavitating flow in centrifugal pumps using multiphase CFD. *J Fluid Eng* 2002;124:377–83.
- [10] Wu Y, Liu S. Simulations of unsteady cavitating turbulent flow in a Francis turbine using the RANS method and the improved mixture model of two-phase flows. *Eng Comput* 2011;27:235–50.
- [11] Liu SH, Zhang L, Nishi M, Wu YL. Cavitating turbulent flow simulation in a Francis turbine based on mixture model. *J Fluids Eng* 2009;131:051302-1–2-8.
- [12] Liu SH, Wu YL, Luo XW. Numerical simulation of 3D cavitating turbulent flow in Francis turbine. In: Proceedings of FEDSM-2005, Houston, FEDSM2005-77017; 2005.
- [13] Pope SB. A more general effective-viscosity hypothesis. *J Fluid Mech* 1975;72(2):331–40.
- [14] Wilcox DC. Re-assessment of the scale-determining equation for advanced turbulence models. *AIAA J* 1988;26(11):1299–310.
- [15] Coutier-Delgosha O, Fortes-Patella R, Reboud JL. Evaluation of the turbulence model influence on the numerical simulations of unsteady cavitation. *Trans ASME* 2003;125:38–45.
- [16] Coutier-Delgosha O, Reboud JL, Albano G. Numerical simulation of the unsteady cavitation behavior of an inducer blade cascade. In: ASME. Proceedings of ASME FEDSM00, New York; 2000.
- [17] Venkateswaran S, Lindau JW, Kunz RF. Computation of multiphase mixture. Flows with compressibility effects. *J Computat Phys* 2002;180:54–77.
- [18] Yan J, Koutnik J, Seidel U. Compressible simulation of rotor–stator interaction in pump–turbines[C]. In: 25th IAHR symposium on hydraulic machinery and systems, vol. 12. Timisoara, Romania; 2012. p. 1–8.
- [19] Okita K, Kajishima T. Numerical simulation of unsteady cavitating flow around a hydrofoil. *Trans JSME B* 2002;68:637–44.